

Journal of Materials Chemistry B

Accepted Manuscript



This is an *Accepted Manuscript*, which has been through the Royal Society of Chemistry peer review process and has been accepted for publication.

Accepted Manuscripts are published online shortly after acceptance, before technical editing, formatting and proof reading. Using this free service, authors can make their results available to the community, in citable form, before we publish the edited article. We will replace this *Accepted Manuscript* with the edited and formatted *Advance Article* as soon as it is available.

You can find more information about *Accepted Manuscripts* in the [Information for Authors](#).

Please note that technical editing may introduce minor changes to the text and/or graphics, which may alter content. The journal's standard [Terms & Conditions](#) and the [Ethical guidelines](#) still apply. In no event shall the Royal Society of Chemistry be held responsible for any errors or omissions in this *Accepted Manuscript* or any consequences arising from the use of any information it contains.

ARTICLE

pH-sensitive perylene bisimide probes for live cell fluorescence lifetime imaging

Cite this: DOI: 10.1039/x0xx00000x

Received 00th January 2012,
Accepted 00th January 2012

DOI: 10.1039/x0xx00000x

www.rsc.org/

D. Aigner^{a*}, R. I. Dmitriev^{b*}, S. M. Borisov^a, D. B. Papkovsky^b and I. Klimant^a

Several new perylene bisimide (PBI) probes comprising oligo-guanidine conjugates and cationic hydrogel nanoparticle structures were designed for sensing intracellular pH in live cell fluorescence lifetime imaging microscopy (FLIM). Using adherent mammalian cells (2D) and neurosphere (3D) cell models, we evaluated their performance by confocal FLIM-TCSPC. The nanoparticle PBI probe showed stable pH calibration and lifetime changes from 4.7 to 3.7 ns between pH 4.4 and 8 attributed to photo-induced electron transfer (PET). The molecular oligo-guanidine probe showed fast cell penetration and bright staining, but its calibration is affected by microenvironment being unreliable for quantitative FLIM. Thus, nanoparticle structures are preferred for design of quantitative pH measurement by FLIM. High brightness and photostability, efficient staining of different cell types and positive optical response to acidification in fluorescence intensity and lifetime modalities are the advantages of the nanoparticle PBI probes compared to conventional pH probes such as BCECF (2',7'-bis-(2-carboxyethyl)-5,6-carboxyfluorescein). Other PBI derivatives with stronger PET can be developed for future high-resolution FLIM of intracellular pH.

Introduction

Intracellular pH in compartmentalized mammalian cells is tightly regulated in complex manner¹. The cytosolic values 7.1 - 7.2 are essential for the function of intracellular organelles. The degradation of proteins in lysosomes requires an acidic pH (4.5 - 5.5)² and the alkaline pH of the mitochondria (7.5 - 8) is crucial for oxidative phosphorylation³⁻⁶. pH gradients play important roles in cell proliferation, senescence and apoptosis⁷, endo- and exocytosis, intracellular transport and organelle recycling^{8, 9}, muscle cell contractility¹⁰ and fluxes of other ions (Na⁺, K⁺, Ca²⁺, Cl⁻)^{1, 5, 6}. Intracellular pH is therefore a useful biomarker for neuroscience^{11, 12}, cancer research, cell bioenergetics and metabolism¹³.

Fluorescence imaging allows the analysis of cells and cellular compartments in multiple dimensions (spatial, temporal, multicolor)¹⁴⁻¹⁶ by means of genetically encoded fluorescent proteins, molecular probes or (polymeric) nanoparticles¹⁷⁻²¹. Such probes can provide fast and efficient loading, bright fluorescent signals and tunable cell-penetrating properties^{22, 23}. The main challenges with synthetic intracellular probes are to achieve their desired localization, stable, specific and robust response to pH and minimal effects by micro-environment on the analytical response. Cell penetration can be achieved using amphiphilic probes with

specific groups and "escort" moieties (e.g. antibody fragments or peptide sequences), or by encapsulating them in cell-permeable polymeric nanoparticles (<100 nm). Current research is focused on new indicator dyes and nanosensors with improved operational performance, bio-distribution and reduced toxicity²⁴⁻³⁰.

The main detection modalities for intracellular pH-probes are fluorescence intensity, (preferably ratiometric detection) and lifetime (FLIM) measurements^{2, 31}. FLIM instrumentation is becoming increasingly popular in biomedical research, since it can provide stable pH calibration and reliable quantitative measurements. FLIM also facilitates multi-parametric analyses, as fluorophores can also be distinguished by their lifetimes. It is also attractive for imaging pH in cultured cells and 3D tissue models³².

The latter was demonstrated with green and red fluorescent proteins³³⁻³⁶, quantum dots^{26, 37} and organic dyes such as 2',7'-bis-(2-carboxyethyl)-5,6-carboxyfluorescein (BCECF), but these probes have non-optimal operational performance and photostability³⁸⁻⁴⁴. There is a clear need in new pH probes with improved brightness, photostability and cell staining properties to make them particularly useful for FLIM applications⁴⁵.

Perylene bisimide (PBI) dyes have convenient spectral properties, bright fluorescence and high photostability⁴⁶⁻⁴⁸. They have been used

for DNA, protein and membrane labeling⁴⁹⁻⁵¹, but not for intracellular pH measurement. The only potential disadvantage of such structures is the high hydrophobicity which requires chemical modification with branched hydrophilic groups to suppress aggregation and non-specific binding⁵²⁻⁵⁶.

In this work, we designed new PBI derivatives for FLIM-based imaging of intracellular pH by introducing amino groups⁵⁷⁻⁵⁹ which cause fluorescence quenching by PET mechanism involving the free amine, but not the protonated form (**Fig. 1**)^{60, 61}. We hypothesized that PET also reduces fluorescence lifetime of the basic form, thus enabling FLIM-based pH imaging. We aimed at moderate effect of PET since strong quenching makes the basic form hard to measure (due to low fluorescent signals) and thus synthesized tetraaryloxy-substituted PBI for which partial PET quenching was previously shown⁵⁸. The solubility, brightness and compatibility with FLIM were improved by incorporating PBI in cationic nanoparticle structures or by chemical modification with guanidine groups which also provide cell-penetrating ability⁶². Both strategies were technically easy to implement, but only the polymeric nanoparticle probe was found suitable for quantitative FLIM measurements. It was superior over the PBI-based molecular probes and also BCECF.

Results and discussion

Preparation and Evaluation of PBI based pH Probes

In this study we designed three different types of PBI probes: anionic PBI, anionic PBI encapsulated in cationic nanoparticles (**NSP**) and anionic PBI with cell penetrating oligoarginine sequences (**MP**) (**Fig. 1**).

(insert Figure 1 here)

The anionic PBI was synthesized by hydrolysis of uncharged precursors using established procedures⁶³. Nanosensor particles (**NSP**) consisted of an anionic PBI derivative incorporated into cationic nanoparticles of Eudragit RL-100[®] hydrogel by precipitation method⁶⁴. This type of nanoparticle vectors is known to provide efficient cell penetration⁶⁵

(insert Figure 2 here)

We evaluated pH sensitivity of **NSP** in aqueous buffer solution (**Fig. 2**) and observed sigmoidal response with a pKa value of 6.4 and lifetime change of ≈ 2 ns, which we attributed to protonation of the amino group and PET¹. Mono-exponential decay fits for PBI (obtained using with 1.2 ns shift, **Fig. S1** in the electronic supplementary information, ESI) were accurate and reproducible, therefore we used them in our study. To see the effect of cellular proteins on fluorescence, **NSP** were measured in the presence of fetal bovine serum (10% and 80%). pH-sensitivity in both fluorescence lifetime and intensity was retained, even though minor effects on the calibration curve were noticed (**Fig. S2**).

In the molecular probe (**MP**) we employed 'branched design'⁶² and introduced four arginine residues by chlorosulfonation followed by the reaction with arginine ethyl ester⁵⁹. For **MP**, fluorescence intensity decreased over a broader pH range (5 – 9), and sigmoidal fits were not applicable. In addition, fluorescence lifetime changed only slightly. Aggregation was evident from diminished quantum

yield (0.33) and altered absorption spectra for tetraaryloxy-PBI⁵⁸. In tetrahydrofuran/water 9:1, the quantum yield was much higher (0.93) and spectra of **MP** were typical for tetraaryloxy-PBI⁵⁸. Thus, aggregation was seen to complicate the pH response of **MP** while it did not occur in **NSP**.

Cell Permeation Properties

Cell permeability of **MP** and **NSP** was studied with mouse embryonic fibroblast (MEF) cells at concentrations of 5 μ M and 10 μ g ml⁻¹ (equivalent to a dye concentration of 0.025 μ M), respectively. **MP** showed faster cell staining, with maximal signals reached at 6 h and 35% of the maximum already after 1 h (**Fig. 3**), but then emission slightly weakened at 24 h of staining. This can be due to hydrolysis of the ester groups in **MP** by cellular esterases changing the net charge and/ or probe migration to a different compartment or microenvironment. Cellular uptake for **NSP** was slower, but emission reached after 24 h was stronger than with **MP**. Slower staining kinetics of **NSP** can be explained by different size and internalization mechanism⁶⁵. Notably, when the cells were stained with anionic PBI probe without polymer shell, the fluorescent signal was > 10 times lower (not shown) and lifetime was practically unaffected by pH ($\Delta\tau \approx 0.3$ ns vs. ≈ 1 ns for **NSP**, **table 1**). This shows the importance of the polymer shell.

(insert Figure 3 here)

Both **NSP** and **MP** in MEF cells displayed punctuated intracellular localization (**Fig. 3**), resembling endosomal compartments^{27, 66}. **NSP** localization showed a considerable overlap with transferrin (marker of clathrin-mediated endosomes including lysosomes, see **Fig. 3**) and no overlap with Dextran 10,000 (macropinosomes) or markers of nuclei and mitochondria (not shown). Lysosomal localization was in agreement with reported for other RL100-based probes⁶⁷. Indeed, when we counter-stained **NSP** with another RL100-PtTPTBPF probe emitting in a different spectral window⁶⁸, we found significant co-localization (yellow color).

We found that **NSP** and **MP** also stained well other adherent cell types such as human colon cancer cells HCT116 (wild type and deficient on oxidative phosphorylation, SCO₂(-/-)⁶⁹) and Caco-2. We observed no damaging or toxic effects after staining for 6 – 20 h. CellTox Green assay (membrane integrity) showed negligible staining after 24 h, and cell viability remained at 98 – 99% (not shown). This data demonstrate that **NSP** and **MP** can be used with different cell types.

Photostability of **NSP** and **MP** was tested and found to be better than conventional pH-probe BCECF and rhodamine derivative TMRM (**Fig. 4**). Upon continuous LED illumination for 2 min, no significant decrease in fluorescent signal was seen, whereas BCECF signal diminished by 30% in the first 10 s. Under these conditions, TMRM signal decreased by $\sim 20\%$ over the whole duration of illumination while **NSP** and **MP** signals remained almost unaffected.

(insert Figure 4 here)

pH Sensing and Imaging with Cultures of Adherent Cells

pH-sensing properties of **NSP** and **MP** were compared with known pH-probe BCECF using FLIM microscopy and cells permeabilized

with nigericin⁷⁰ and equilibrated in buffer solutions of different pH spanning the physiological range (4.4 – 8)¹ (**Fig. 5, S3** and **table 1**). For **NSP**, the changes in lifetime ($\Delta\tau$) were less profound (~1 ns), than in plain buffer (≈ 2 ns) and varied slightly for different cell lines (**table 1**). Variations in fluorescence lifetime within individual images were significant. The distribution of absolute lifetime values was broader for **NSP** (half-width 0.3 – 0.6 ns) than for BCECF (0.2 – 0.3 ns), but its relative variation was narrower (25 – 65%, compared to 100 – 150% for BCECF, $\Delta\tau$ was 0.9 – 1.2 ns for **NSP** and ≈ 0.2 ns for BCECF).

(Insert Table 1 here)

Hence, **NSP** provide better resolution in pH measurements by FLIM. For **MP**, which lacks a protective polymer shell, $\Delta\tau$ in cells (0.5 – 1 ns) was larger than in buffer (0.3 ns), depended strongly on the cell type, and showed broad distributions of lifetimes (**table 2, Fig. 5, S3**). Even though pH affected probe lifetime, we were unable to perform pH calibrations reliably due to considerable variability of results and effects of probe microenvironment.

Reported in literature $\Delta\tau$ for BCECF was typically 0.5 – 1 ns, though absolute values for the acidic and basic forms varied significantly³⁸⁻⁴¹. A smaller $\Delta\tau$, comparable to our data was recently reported by Hille et al⁷¹. Although BCECF emission intensity did change with pH (decreased at acidic pH, **Fig. S4**), lifetime response was poor (0.2 – 0.3 ns). Overall, **NSP** clearly displays a better resolution in pH imaging by FLIM.

(insert Figure 5 here)

pH calibrations for **NSP** for MEF and HCT116 $\text{SCO}_2(-/-)$ cells in FLIM mode shown in **Fig. 5C** are similar to calibration obtained in buffer. For the range pH 4.4 – 6, a linear fit can be used. At temperatures 25 °C the calibration differed significantly from 37°C (**Fig. S5**), but linear fits were still applicable. In buffer, lifetime calibrations at 37 °C and 25 °C were similar (**Fig. S5**).

The lifetime observed with **NSP** in resting cells indicated low pH values (5.4 in MEF, 5.2 in HCT116, at 25 °C), which corresponds to probe localization in acidic organelles such as recycling endosomes and lysosomes^{67, 72}. This can be used for studying of drug effects on acidic organelles such as lysosomes. Indeed, when we treated resting MEF cells with a drug affecting lysosomal acidification (bafilomycin A1) which leads to rapid (15 – 30 min) inhibition of V-ATPase and increase of lysosomal pH⁷³, we found a consistent decrease in **NSP** lifetime for the same regions of interest (**Fig. S6**) and the disappearance of LysoTracker Red staining (not shown). The observed decrease of 0.2 – 0.3 ns corresponds to an increase in pH by 0.9 units, with respect to the initial value (pH = 4.7).

Collectively, our data indicates that **NSP** can be used for sensing pH in acidic organelles in conventional (2D) cell cultures.

Application of PBI Probes for FLIM Imaging of Multi-cellular Spheroid (3D) Models

Physiological experiments become more relevant when the cells maintain cell-cell interactions in 3D environment and experience diffusion-limited supply of metabolites⁷⁴. We therefore tested **NSP** and **MP** with neurospheres - heterogeneous multi-cellular spheroid aggregates 0.1 – 0.5 mm in size. Neurosphere model is widely used

to study processes of neural cell development, cellular responses to various patho-physiological conditions and drugs in 3D^{75, 76}.

Using a previously optimized procedure⁷⁷, we produced neurospheres from rat embryonic brain and stained them with BCECF, **NSP** and **MP**. Notably, **NSP** and **MP** displayed efficient in-depth staining, while BCECF produced weak signals in neurosphere interior which can indicate either inefficient probe accumulation or lower pH values in the core (**Fig. 6**). Based on average values from 3 spheroids of 0.2 – 0.3 mm diameter, **MP** yielded 2.1-fold higher signals than **NSP** and 5.2-fold higher than BCECF.

(insert Figure 6 here)

Analysis of **NSP** distribution across the spheroids revealed extracellular patch-like localization, similar to the other RL100-based probes^{77, 78}. FLIM analysis revealed the presence of regions inside the spheroids with decreased lifetime (~0.6 ns), i.e. increased pH (**Fig. 6B**). These “alkaline” cores were of asymmetrical shape and present in several regions of the spheroid. They can also indicate functional cell heterogeneity of neurosphere-forming cells. This is different from the data for tumor spheroids⁷⁶ and can be explained by the different nature of neurosphere-forming cells (neural stem cells) and their metabolism¹³

To see if the pH inside the neurospheres is dynamically regulated, we stimulated neurospheres with sodium glutamate, a common neuromediator and excitotoxic stimulant⁷⁹. **Fig. 6C** shows profound and reproducible decrease of fluorescence lifetime within 15 – 30 min, implying alkalization in extracellular regions of neurospheres. Thus, our experiments demonstrate that PBI can be used for pH mapping and time-lapse monitoring by FLIM within spheroid cultures.

Experimental

Materials and Methods

Calcein Green AM, BCECF, tetramethylrhodamine methyl ester (TMRM), B27 serum-free supplement, Alexa Fluor 488-dextran 10,000 and transferrin conjugates, MitoTracker Green were from Invitrogen (Biosciences, Dublin, Ireland). Epidermal growth (EGF) and fibroblast growth (FGF) factors were from Millipore (Cork, Ireland). PtTPTBPF-RL100 nanoparticles were prepared as described previously⁸⁰. CellTox Green Cytotoxicity assay kit was from Promega (MyBio, Ireland). 1,6,7,12-Tetrachloroperylene-3,4:9,10-tetracarboxylic bisanhydride was from Beijing Wenhaiyang Industry and Trading Co. Ltd (<http://china.zhaoteng.com>), 1-methyl-2-pyrrolidone from TCI Europe (<http://www.tcichemicals.com>). Deuterated solvents were obtained from Eurisotop (www.eurisotop.com), silica gel from Acros (www.fishersci.com). Eudragit® RL100 was from Evonik Industries (<http://corporate.evonik.de>). All other chemicals and reagents were from Sigma-Aldrich. Standard cell culture grade plasticware was from Sarstedt (Wexford, Ireland) and Corning (VWR, Ireland), glass bottom mini-dishes were from MatTek (Ashland, USA), glass bottom multiwell slides from Ibidi (Martinsried, Germany). NMR spectra were recorded on a 300 MHz instrument (Bruker) with TMS as a standard. MALDI-TOF mass spectra were taken on a

Micromass TofSpec 2E in reflectron mode at an accelerating voltage of +20 kV. Absorption measurements were performed on a Cary 50 UV-VIS spectrophotometer from Varian (www.varianinc.com). Fluorescence spectra were recorded on a Hitachi F-7000 spectrofluorimeter (www.hitachi.com). Relative fluorescence quantum yields were determined at 25 °C using rhodamine 101 ($\Phi_F = 0.98$ in ethanol) as a standard.

Dye Syntheses

N-(2,6-Diisopropylphenyl)-N'-(2-dimethylaminoethyl)-1,6,7,12-tetraphenoxyperylene-3,4:9,10-tertracarboxylic bisimide (2): 1,6,7,12-Tetrachloroperylene-3,4:9,10-tertracarboxylic bisanhydride (3 g, 5.66 mmol) was dissolved in 1-methyl-2-pyrrolidone (NMP; 210 ml) at 80°C. A solution of 648 μ l (5.66 mmol) *N,N*-dimethylethylenediamine in NMP (10 ml) was added dropwise and the mixture stirred for 1 h. Temperature was increased to 120°C, 2,6-diisopropylaniline (4.61 ml, 22.7 mmol) and propionic acid (70 ml) were added and the mixture was stirred overnight. The crude product was precipitated with 20% aqueous sodium chloride solution, filtered, washed with water and dried. Purification by column chromatography (Silica gel 40-63 μ m) with dichloromethane/methanol 40:1 (V/V) as eluent afforded 1.58 g (37%) *N*-(2,6-diisopropylphenyl)-*N'*-(2-dimethylaminoethyl)-1,6,7,12-tetrachloroperylene-3,4:9,10-tertracarboxylic bisimide; ^1H NMR: (300 MHz, CDCl_3), δ : 8.71 (2s, 4H, perylene ArH), 7.52 (t, $J = 7.8$ Hz, 1H, ArH), 7.38 (d, $J = 7.7$ Hz, 2H, ArH), 4.39 (t, $J = 6.3$ Hz, 2H, $\text{NCH}_2\text{CH}_2\text{N}(\text{CH}_3)_2$), 2.6 – 2.8 (m, 4H, $\text{ArCH}(\text{CH}_3)_2$ and $\text{NCH}_2\text{CH}_2\text{N}(\text{CH}_3)_2$), 2.37 (s, 6H, $\text{N}(\text{CH}_3)_2$), 1.18 (dd, $J_1 = 3.7$ Hz, $J_2 = 3.2$ Hz, 12H, $\text{ArCH}(\text{CH}_3)_2$). ^{13}C -APT NMR-spectrum (300MHz, CDCl_3), δ : 162.4 (C=O), 145.6, 133.5, 133.4 (perylene C(Ar)-H), 133.1 (perylene C(Ar)-H), 130.0 (C(Ar)-H), 129.0, 128.6, 124.3 (C(Ar)-H), 123.4, 123.1; 57.0 ($\text{NCH}_2\text{CH}_2\text{N}(\text{CH}_3)_2$), 45.8 ($\text{N}(\text{CH}_3)_2$), 38.5 ($\text{NCH}_2\text{CH}_2\text{N}(\text{CH}_3)_2$), 29.3 ($\text{ArCH}(\text{CH}_3)_2$), 24.0 ($\text{ArCH}(\text{CH}_3)_2$). MALDI-TOF: m/z [M^+] 760.1169 found, 760.1125 calcd.

800 mg (1.05 mmol) of the obtained product, phenol (950 mg, 10.1 mmol), potassium carbonate (1.1 g, 7.96 mmol) and NMP (60 ml) were stirred at 115°C for 6 h. The crude product was precipitated with 20% aqueous sodium chloride solution containing 0.3 M HCl, filtered, washed with water, dried and purified by column chromatography (silica gel 40 – 63 μ m) with dichloromethane / methanol 50:1 (V/V) as eluent, yield 0.78 g (75 %) of compound **2**. ^1H NMR: (300 MHz, CDCl_3), δ : 8.21 (2s, 4H, perylene ArH), 7.42 (t, $J = 7.8$ Hz, 1H, ArH), 7.20 – 7.33 (m, 10H, ArH), 7.12 (q, $J = 7.8$ Hz, 4H, ArH), 6.96 (q, $J = 3.9$ Hz, 8H, ArH), 4.28 (t, $J = 6.8$ Hz, 2H, $\text{NCH}_2\text{CH}_2\text{N}(\text{CH}_3)_2$), 2.58 – 2.75 (m, 4H, $\text{ArCH}(\text{CH}_3)_2$ and $\text{NCH}_2\text{CH}_2\text{N}(\text{CH}_3)_2$), 2.34 (s, 6H, $\text{N}(\text{CH}_3)_2$), 1.12 (d, $J = 6.8$ Hz, 12H, $\text{ArCH}(\text{CH}_3)_2$). ^{13}C -APT NMR-spectrum (300MHz, CDCl_3), δ : 163.2 (C=O), 155.9, 155.2, 145.6, 133.4, 133.0, 130.7, 130.0 (C(Ar)-H), 129.5 (C(Ar)-H), 124.6 (C(Ar)-H), 123.9 (perylene C(Ar)-H), 122.8, 122.7, 120.8, 120.5, 120.4 (C(Ar)-H), 120.0 (C(Ar)-H), 119.8; 56.9 ($\text{NCH}_2\text{CH}_2\text{N}(\text{CH}_3)_2$), 45.6 ($\text{N}(\text{CH}_3)_2$), 38.2 ($\text{NCH}_2\text{CH}_2\text{N}(\text{CH}_3)_2$), 29.1 ($\text{ArCH}(\text{CH}_3)_2$), 24.0 ($\text{ArCH}(\text{CH}_3)_2$). MALDI-TOF: m/z [M^+] 990.3752 found, 990.3754 calcd.

N-(2,6-Diisopropyl-4-sulfophenyl)-N'-(2-dimethylaminoethyl)-1,6,7,12-tetra(4-sulfophenoxy)perylene-3,4:9,10-tertracarboxylic bisimide (3) and

N-(2,6-Diisopropyl-4-([N-(1-ethoxycarbonyl-4-guanidinybutyl)amino]sulfonyl)phenyl)-N'-(2-dimethylaminoethyl)-1,6,7,12-tetra(4-([N-(1-ethoxycarbonyl-4-guanidinybutyl)amino]sulfonyl)phenoxy)perylene-3,4:9,10-tertracarboxylic bisimide (MP): Compound **2** (200 mg, 0.202 mmol) in 3 ml chlorosulfonic acid was stirred at 0°C for 50 min, added dropwise onto ice cubes, filtered, washed with cold water and dried under vacuum at RT to yield the sulfochloride intermediate (298 mg), which was used without further purification. ^1H NMR (300 MHz, CDCl_3 , TMS), δ : 8.71 (2s, 4H, ArH); 7.52 (t, $J = 7.6$ Hz, 1H, ArH); 7.38 (d, $J = 7.7$ Hz, 2H, ArH); 4.41 (t, $J = 5.7$ Hz, 2H, CH_2); 2.76 (m, 4H, CH, CH_2); 2.42 (s, 6H, CH_3); 1.18 (dd, $J_1 = 3.7$ Hz, $J_2 = 3.2$ Hz, 12H, CH_3).

For the preparation of **3**, 150 mg of the sulfochloride was stirred overnight in a mixture of tetrahydrofuran (8 ml), water (2 ml) and triethylamine (200 μ l, 1.43 mmol). The mixture was concentrated under vacuum and purified by column chromatography (silica gel 40 – 63 μ m) with dichloromethane/methanol 3:1 (V/V) as eluent. The product was re-dissolved in a mixture of methanol (0.5 ml) and water (0.1 ml) and precipitated with a mixture of methylene chloride, toluene and n-hexane (1 ml each) to yield 68 mg (52 %) of deep red powder after drying.

^1H NMR (300MHz, $\text{CD}_3\text{OD}:\text{D}_2\text{O}$ 3:1 (V/V)), δ : 8.19 (2H, s, perylene ArH), 8.07 (2H, s, perylene ArH), 7.81 (4H, d, $J = 8.7\text{Hz}$, ArH), 7.68 (4H, d, $J = 8.7\text{Hz}$, ArH), 7.44 (1H, t, $J = 7.6\text{Hz}$, ArH), 7.31 (2H, d, $J = 7.8\text{Hz}$, ArH), 7.05 (8H, 2d, ArH), 4.49 (2H, broad s, $\text{NCH}_2\text{CH}_2\text{N}(\text{CH}_3)_2$), 3.51 (2H, broad s, $\text{NCH}_2\text{CH}_2\text{N}(\text{CH}_3)_2$), 3.00 (6H, s, $\text{N}(\text{CH}_3)_2$), 2.67 (2H, m, $\text{ArCH}(\text{CH}_3)_2$), 1.09 (12H, d, $J = 6.7\text{Hz}$, $\text{ArCH}(\text{CH}_3)_2$). ^{13}C -APT NMR (300MHz, $\text{CD}_3\text{OD}:\text{D}_2\text{O}$ 3:1 (V/V)), δ : 164.9 (C=O), 158.4, 158.2, 156.6, 156.1, 147.2, 142.7, 142.6, 131.1 (C(Ar)-H), 129.4 (C(Ar)-H), 125.1 (C(Ar)-H), 124.4, 122.9 (perylene C(Ar)-H), 122.4 (perylene C(Ar)-H), 122.2, 122.0, 120.0 (C(Ar)-H); 58.0 ($\text{NCH}_2\text{CH}_2\text{N}(\text{CH}_3)_2$), 44.4 ($\text{N}(\text{CH}_3)_2$), 37.3 ($\text{NCH}_2\text{CH}_2\text{N}(\text{CH}_3)_2$), 30.3 ($\text{ArCH}(\text{CH}_3)_2$), 24.3 ($\text{ArCH}(\text{CH}_3)_2$). HRMS: m/z 1310.20 ($[\text{MH}^+]$), 1310.20 calcd.; 1332.19 ($[\text{MNa}^+]$), 1332.18 calcd.; 1348.16 ($[\text{MNaK}^+]$), 1348.16 calcd.). UV-vis (H_2O): λ_{max} (ϵ) = 567 (32000), 536 (32000), 454 nm (17000).

For the preparation of **MP**, the rest of the sulfochloride was added to a solution of arginine ethyl ester dihydrochloride (275 mg, 1.00 mmol) and triethylamine (290 μ l, 2.07 mmol) in dry *N,N*-dimethylformamide (10 ml) and stirred overnight at RT. The crude product was precipitated and washed with 20% aqueous sodium chloride solution, dried and purified by HPLC chromatography (column NUCLEODUR® 100-5 C18 ec, 125 mm \times 21mm ID, Macherey-Nagel, on a Dionex™ UltiMate™ 3000 semi-preparative system) as stated in detail in **table S1**, yield 19 mg (8%). ^1H NMR: (300 MHz, CD_3OD), δ : 8.19 (d, $J = 8.4\text{Hz}$, 4H, ArH), 7.81 (dd, $J_1 = 6.2\text{Hz}$, $J_2 = 8.5\text{Hz}$, 8H, ArH), 7.45 (t, $J = 7.8\text{Hz}$, 1H, ArH), 7.30 (d, $J = 7.6\text{Hz}$, 2H, ArH), 7.12 (dd, $J_1 = 8.6\text{Hz}$, $J_2 = 16.5\text{Hz}$, 8H, ArH), 4.50 (broad s, 2H, CH_2), 3.85 – 4.10 (m, 12H, CH and CH_2), 3.51 (broad s, 2H, CH_2), 3.22 (m, 8H, CH_2), 2.97 (s, 6H, CH_3), 2.69 (p, J

= 6.8 Hz, 2H, CH), 1.6 – 1.9 (m, 16H, CH₂), 1.0 – 1.23 (m, 24H, CH₃). ¹³C-APT NMR (300 MHz, CD₃OD) δ: 172.7 (COOR), 164.6 (C=O), 160.5, 160.2, 156.1, 155.8, 147.2, 138.2, 131.7, 130.9 (C(Ar)-H), 130.8 (C(Ar)-H), 125.2, 125.1 (C(Ar)-H), 124.7, 122.7 (perylene C(Ar)-H), 122.5, 120.6 (C(Ar)-H); 62.7 (O-CH₂-CH₃), 57.0 (N-CH₂-CH₂-N(CH₃)₂), 56.9 (CH), 44.6 (N(CH₃)₂), 41.7 (CH₂-NH), 37.0 ((N-CH₂-CH₂-N(CH₃)₂), 31.1 (CH₂), 30.3 (Ar-CH(CH₃)₂), 26.1 (CH₂), 24.3 (Ar-CH(CH₃)₂), 14.5 (O-CH₂-CH₃). HRMS: *m/z* 2046.72 ([MH⁺], 2046.73 calcd.). UV-vis (*H*₂O): λ_{max} (ε) = 557 (42000), 447 nm (17000).

Preparation of Nanosensor Particles (NSP)

This was done accordingly to previously described procedure⁸⁰. Briefly, a solution of RL100 polymer (200 mg) and **3** (0.5 mg) in acetone (80 ml) was prepared and water (500 ml) was added quickly (5 s). The nanoparticle suspension (typical average size 30 nm) was concentrated in vacuum to reach a concentration of 5 g l⁻¹ and was stored at 4°C (1 month). Prior the use, it was filtered through 0.2 μm filter.

Cell Culture

Mouse embryonic fibroblast (MEF), human colon carcinoma HCT116 and human colorectal adenocarcinoma Caco-2 cells were from ATCC (Manassas, VA, USA) and were handled as described previously⁷⁸. For fluorescence microscopy and confocal imaging, cells were seeded for onto Cell⁺ (confocal upright microscope) or glass bottom (inverted microscope) collagen-poly-D-lysine coated mini-dishes to reach 50 – 75% confluence. Staining with fluorescent probes was performed by addition of medium containing probe, incubation (0.5 – 24 h) and 1 – 2 cycles of washing. Typical staining concentrations/times for fluorescent probes were 2.5 μM/ 0.5 h (BCECF), 20 nM/ 10 min (TMRM), 1 μM/ 0.5 h (Hoechst 33342, Calcein Green AM), 0.01%/ 10 min (CellTox Green), 25 μg ml⁻¹/ 0.5 h (Dextran 10,000-Alexa Fluor488), 40 μg ml⁻¹/ 0.5 h (Transferrin-AlexaFluor488), 100 nM/ 0.5 h (MitoTracker Green), 10 μg ml⁻¹/ 16 h (PtTPTBPF in RL100).

Neurosphere Culture

All procedures with animals were performed under a licence issued by the Irish Government Department of Health and Children (Ireland) and in accordance with the Directive 2010/63/EU adopted by the European Parliament and the Council of the European Union. Neurospheres from cortices of embryonic (E18) rat brain were prepared as described before⁷⁷ and cultured in DMEM/ F12 Ham medium supplemented with FGF (20 ng ml⁻¹), EGF (20 ng ml⁻¹), B27 (2%) and penicillin-streptomycin for 4 days in vitro (DIV), to reach a size of 0.1 – 0.5 mm. For microscopy, neurospheres were collected, washed with medium and plated on poly-D-lysine coated 35 mm dishes and allowed to adhere for 30 min.

Microscopy

Analysis of cell staining kinetics, cell viability and photostability experiments were performed on wide-field fluorescence microscope Axiovert 200 (Zeiss) equipped with custom made pulsed LED (390, 470 and 590 nm excitation), fluorescence emission filter cubes and integrated temperature and CO₂/O₂ control as described previously⁷⁷.

FLIM imaging was performed on upright Axio Examiner Z1 (Zeiss) microscope, equipped with 20x/1.0 W Apochromat objective, heated stage (Z-axis control), integrated TCSPC (time-correlated single photon counting) confocal scanning module DCS-120 (Becker & Hickl, Germany), an R10467U-40 and 50 photon counting detectors (Hamamatsu Photonics K.K.) and TCSPC hardware (Becker & Hickl)⁷⁷. The PBI and TMRM probes were excited with picosecond supercontinuum laser SC400-4 (Fianium, UK) at 540 nm (561 nm longpass filter, emission 565 – 605 nm), while BCECF, Calcein Green, Alexa Fluor 488-conjugates and MitoTracker Green at 488 nm (495 nm longpass filter, emission 512 – 536 nm). Hoechst 33342 probe was excited at 405 nm (435 nm longpass filter, emission 438 – 458 nm). PtTPTBPF in RL100 was excited at 614 nm (665 nm longpass filter, emission 750-810 nm).

Buffers for pH titrations used were composed of 10 mM buffer salt (sodium acetate, MES, MOPS or HEPES), 135 mM KCl, 2 mM CaCl₂, 1 mM MgCl₂ and 20 mM Sucrose. Prior to calibration, nigericin (10 μM) was added with 15 – 30 min pre-incubation time. The following equation was used for sigmoidal calibration:

$$I = \frac{A_{\min} - A_{\max}}{1 + e^{(pH - pK_a)/dx}} + A_{\max}$$

where *I* - fluorescence intensity, *A*_{max}, *A*_{min}, and *dx* are numerical coefficients.

Data processing

The wide-field microscopy imaging data were processed in ImSpector pro software (La Vision BioTec, Germany), and exported in ASCII (line profiles) or RGB TIFF (images) format. FLIM data obtained from 256x256 regions of interest were fit using mono-exponential decay function, delay parameter *t*₁=42, binning factor 1 in SPCImage software (Becker & Hickl). Fit curves in each pixel, excluding dark regions, yielded a lifetime distribution over the whole image, with lifetime being displayed on the x-axis and the abundance of each lifetime on the y-axis. From the distribution curve were calculated the average lifetime (50% of the total integral is reached) and half-width (difference between lifetimes at which half-maximal abundance is reached).

Conclusions

We have presented new pH FLIM probes based on perylene bisimides, either immobilized in cationic hydrogel particles (NSP) or conjugated to cell-penetrating moieties (MP). We found NSP as most suitable for intracellular pH measurements by FLIM, as it provided most reliable lifetime calibration (specific for different cell types). This probe displayed predominantly lysosomal staining within 6 – 24 h, similarly to other nanoparticle pH probes reported before²⁷. High photostability and brightness and better lifetime resolution are the advantages over conventional molecular probes such as BCECF or fluorescent proteins. NSP was demonstrated in FLIM measurements with four different cell lines (2D cell culture) and spheroids from primary neural cells (3D culture). Further optimization and improvement of pH-resolution can be achieved by

increasing the efficiency of the PET process with different PET groups and/or PBI structures.

In comparison to **NSP**, the molecular probe **MP** was not useful for intracellular pH-measurement by FLIM, due to unstable calibration, aggregation and effects of cellular components. Thus, nanoparticle structures feature significant advantages in design of FLIM-based pH-probes, compared to "unprotected" small molecule and fluorescent protein probes.

Acknowledgements

This work was supported by Science Foundation Ireland (SFI) grants 12/TIDA/B2413 and 12/RC/2276 and by Graz University of Technology travel grant "Förderungsstipendium für wissenschaftliche Arbeiten 2013". We thank Alina Kondrashina (University College Cork) for preparation of PtTPTBPF nanoparticles and Tara Foley (University College Cork) for help with isolation of primary neurons, as well as Becker & Hickl GmbH for providing software licenses, the Nano-optics Department, Institute of Physics, Karl-Franzens University Graz, for help with preliminary TCSPC experiments, Robert Saf (Institute of Chemistry and Technology of Materials, Graz University of Technology) for HRMS-measurements and Gernot Strohmeier (Institute of Organic Chemistry, Graz University of Technology) for support with HPLC purification.

Notes and references

AFFILIATIONS:

^a Institute of Analytical Chemistry and Food Chemistry, Graz University of Technology, NAWI Graz, Stremayrgasse 9, Graz, Austria. Tel.: +4331687332514. E-Mail: daigner@tugraz.at

^b School of Biochemistry and Cell Biology, University College Cork, Cork, Ireland. E-mail: r.dmitriev@ucc.ie

† * Authors contributed equally to this work.

ABBREVIATIONS: FLIM - fluorescence lifetime imaging microscopy; LED - light emitting diode; PBI - perylene bisimide; PET - photoinduced electron transfer; TCSPC - time-correlated single photon counting;

Electronic Supplementary Information (ESI) available: Supporting Information contains additional figures S1-S6, HPLC purification protocol and structure confirmation of synthesized compounds (S7-S21).

See DOI: 10.1039/b000000x/

- J. R. Casey, S. Grinstein and J. Orłowski, *Nature reviews Molecular cell biology*, 2009, **11**, 50-61.
- J. Han and K. Burgess, *Chemical reviews*, 2009, **110**, 2709-2728.
- M. F. C. Abad, G. Di Benedetto, P. J. Magalhães, L. Filippin and T. Pozzan, *Journal of Biological Chemistry*, 2004, **279**, 11521-11529.
- J. Llopis, J. M. McCaffery, A. Miyawaki, M. G. Farquhar and R. Y. Tsien, *Proceedings of the National Academy of Sciences*, 1998, **95**, 6803-6808.
- J. Shin, K. Munson, O. Vagin and G. Sachs, *Pflugers Arch - Eur J Physiol*, 2009, **457**, 609-622.
- M. Numata and J. Orłowski, *Journal of Biological Chemistry*, 2001, **276**, 17387-17394.
- D. Pérez-Sala, D. Collado-Escobar and F. Mollinedo, *Journal of Biological Chemistry*, 1995, **270**, 6235-6242.
- F. R. Maxfield and T. E. McGraw, *Nat Rev Mol Cell Biol*, 2004, **5**, 121-132.
- J. Gruenberg and H. Stenmark, *Nat Rev Mol Cell Biol*, 2004, **5**, 317-323.
- E. R. Chin and D. G. Allen, *The Journal of Physiology*, 1998, **512**, 831-840.
- M. Chesler, *Physiological reviews*, 2003, **83**, 1183-1221.
- J. W. Deitmer and C. R. Rose, *Progress in Neurobiology*, 1996, **48**, 73-103.
- B. A. Webb, M. Chimenti, M. P. Jacobson and D. L. Barber, *Nature Reviews Cancer*, 2011, **11**, 671-677.
- J. R. Lakowicz, *Principles of fluorescence spectroscopy*, Springer, 2007.
- M. Schäferling, *Angewandte Chemie International Edition*, 2012, **51**, 3532-3554.
- A. M. Powe, S. Das, M. Lowry, B. El-Zahab, S. O. Fakayode, M. L. Geng, G. A. Baker, L. Wang, M. E. McCarroll, G. Patonay, M. Li, M. Aljarrah, S. Neal and I. M. Warner, *Analytical chemistry*, 2010, **82**, 4865-4894.
- P. Dedecker, F. C. De Schryver and J. Hofkens, *Journal of the American Chemical Society*, 2013, **135**, 2387-2402.
- K. Nienhaus and G. U. Nienhaus, *Chemical Society Reviews*, 2014.
- D. M. Shcherbakova, O. M. Subach and V. V. Verkhusha, *Angewandte Chemie International Edition*, 2012, **51**, 10724-10738.
- R. P. Haugland, *The handbook: a guide to fluorescent probes and labeling technologies*, Molecular probes, 2005.
- X. Li, X. Gao, W. Shi and H. Ma, *Chemical reviews*, 2013, **114**, 590-659.
- E. C. Jensen, *The Anatomical Record: Advances in Integrative Anatomy and Evolutionary Biology*, 2012, **295**, 2031-2036.
- B. N. G. Giepmans, S. R. Adams, M. H. Ellisman and R. Y. Tsien, *science*, 2006, **312**, 217-224.
- S. M. Borisov and I. Klimant, *Analyst*, 2008, **133**, 1302-1307.
- R. Singh and H. S. Nalwa, *Journal of biomedical nanotechnology*, 2011, **7**, 489-503.
- A. M. Dennis, W. J. Rhee, D. Sotto, S. N. Dublin and G. Bao, *ACS nano*, 2012, **6**, 2917-2924.
- R. V. Benjaminsen, H. Sun, J. R. Henriksen, N. M. Christensen, K. Almdal and T. L. Andresen, *ACS nano*, 2011, **5**, 5864-5873.
- A. Ray, Y. E. K. Lee, G. Kim and R. Kopelman, *Small*, 2012, **8**, 2213-2221.
- M. Schäferling, R. Arppe, T. Soukka, S. Nylund, L. Mattsson, S. Koho, J. Rosenholm and T. Näreoja, *Nanoscale*, 2014.
- W. Shi, X. Li and H. Ma, *Angewandte Chemie International Edition*, 2012, **51**, 6432-6435.

31. M. Y. Berezin and S. Achilefu, *Chemical reviews*, 2010, **110**, 2641-2684.
32. W. Becker, *Journal of Microscopy*, 2012, **247**, 119-136.
33. M. Tantama, Y. P. Hung and G. Yellen, *Journal of the American Chemical Society*, 2011, **133**, 10034-10037.
34. A. Battisti, M. A. Digman, E. Gratton, B. Storti, F. Beltram and R. Bizzarri, *Chemical Communications*, 2012, **48**, 5127-5129.
35. T. Nakabayashi, S. Oshita, R. Sumikawa, F. Sun, M. Kinjo and N. Ohta, *Journal of Photochemistry and Photobiology A: Chemistry*, 2012, **235**, 65-71.
36. A. Esposito, M. Gralle, M. A. C. Dani, D. Lange and F. S. Wouters, *Biochemistry*, 2008, **47**, 13115-13126.
37. A. Orte, J. M. Alvarez-Pez and M. J. Ruedas-Rama, *ACS nano*, 2013, **7**, 6387-6395.
38. R. Niesner, B. Peker, P. Schlüsche, K.-H. Gericke, C. Hoffmann, D. Hahne and C. Müller-Goymann, *Pharm Res*, 2005, **22**, 1079-1087.
39. C. Hille, M. Berg, L. Bressel, D. Munzke, P. Primus, H.-G. Löhmansröben and C. Dosche, *Anal Bioanal Chem*, 2008, **391**, 1871-1879.
40. H.-P. Wang, T. Nakabayashi, K. Tsujimoto, S. Miyauchi, N. Kamo and N. Ohta, *Chemical physics letters*, 2007, **442**, 441-444.
41. K. M. Hanson, M. J. Behne, N. P. Barry, T. M. Mauro, E. Gratton and R. M. Clegg, *Biophysical Journal*, 2002, **83**, 1682-1690.
42. H. J. Lin, P. Herman and J. R. Lakowicz, *Cytometry Part A*, 2003, **52**, 77-89.
43. M. Hassan, J. Riley, V. Chernomordik, P. Smith, R. Pursley, S. B. Lee, J. Capala and A. H. Gandjbakhche, *Molecular imaging*, 2007, **6**, 229.
44. H. Szmazinski and J. R. Lakowicz, *Analytical chemistry*, 1993, **65**, 1668-1674.
45. O. S. Wolfbeis, *Angewandte Chemie International Edition*, 2013, **52**, 9864-9865.
46. A. Rademacher, S. Märkle and H. Langhals, *Chemische Berichte*, 1982, **115**, 2927-2934.
47. T. Weil, T. Vosch, J. Hofkens, K. Peneva and K. Müllen, *Angewandte Chemie International Edition*, 2010, **49**, 9068-9093.
48. F. Wurthner, *Chemical Communications*, 2004, 1564-1579.
49. K. Peneva, G. Mihov, A. Herrmann, N. Zarrabi, M. Börsch, T. M. Duncan and K. Müllen, *Journal of the American Chemical Society*, 2008, **130**, 5398-5399.
50. K. Peneva, G. Mihov, F. Nolde, S. Rocha, J.-i. Hotta, K. Braeckmans, J. Hofkens, H. Uji-i, A. Herrmann and K. Müllen, *Angewandte Chemie International Edition*, 2008, **47**, 3372-3375.
51. C. Jung, B. K. Müller, D. C. Lamb, F. Nolde, K. Müllen and C. Bräuchle, *Journal of the American Chemical Society*, 2006, **128**, 5283-5291.
52. H. Liu, Y. Wang, C. Liu, H. Li, B. Gao, L. Zhang, F. Bo, Q. Bai and X. Ba, *Journal of Materials Chemistry*, 2012, **22**, 6176-6181.
53. S. K. Yang, X. Shi, S. Park, S. Doganay, T. Ha and S. C. Zimmerman, *Journal of the American Chemical Society*, 2011, **133**, 9964-9967.
54. M. Yin, J. Shen, R. Gropeanu, G. O. Pflugfelder, T. Weil and K. Müllen, *Small*, 2008, **4**, 894-898.
55. C. D. Schmidt, C. Böttcher and A. Hirsch, *European Journal of Organic Chemistry*, 2009, **2009**, 5337-5349.
56. T. Heek, C. Fasting, C. Rest, X. Zhang, F. Wurthner and R. Haag, *Chemical Communications*, 2010, **46**, 1884-1886.
57. L. M. Daffy, A. P. de Silva, H. Gunaratne, C. Huber, P. Lynch, T. Werner and O. S. Wolfbeis, *Chemistry-A European Journal*, 1998, **4**, 1810-1815.
58. D. Aigner, S. Borisov and I. Klimant, *Anal Bioanal Chem*, 2011, **400**, 2475-2485.
59. D. Aigner, S. M. Borisov, P. Petritsch and I. Klimant, *Chemical Communications*, 2013, **49**, 2139-2141.
60. R. A. Bissell, A. P. de Silva, H. Q. N. Gunaratne, P. L. M. Lynch, G. E. M. Maguire and K. R. A. S. Sandanayake, *Chemical Society Reviews*, 1992, **21**, 187-195.
61. A. P. de Silva, T. P. Vance, M. E. S. West and G. D. Wright, *Organic & Biomolecular Chemistry*, 2008, **6**, 2468-2480.
62. R. I. Dmitriev, H. Ropiak, G. Ponomarev, D. V. Yashunsky and D. B. Papkovsky, *Bioconjugate Chemistry*, 2011, **22**, 2507-2518.
63. C. Kohl, T. Weil, J. Qu and K. Müllen, *Chemistry – A European Journal*, 2004, **10**, 5297-5310.
64. S. M. Borisov, T. Mayr, G. Mistlberger, K. Waich, K. Koren, P. Chojnacki and I. Klimant, *Talanta*, 2009, **79**, 1322-1330.
65. A. Fercher, S. M. Borisov, A. V. Zhdanov, I. Klimant and D. B. Papkovsky, *ACS nano*, 2011, **5**, 5499-5508.
66. K. Koren, R. I. Dmitriev, S. M. Borisov, D. B. Papkovsky and I. Klimant, *ChemBioChem*, 2012, **13**, 1184-1190.
67. R. I. Dmitriev, A. V. Zhdanov, G. Jasionek and D. B. Papkovsky, *Analytical chemistry*, 2012, **84**, 2930-2938.
68. S. Borisov, G. Nuss, W. Haas, R. Saf, M. Schmuck and I. Klimant, *Journal of Photochemistry and Photobiology A: Chemistry*, 2009, **201**, 128-135.
69. H. J. Sung, W. Ma, P.-y. Wang, J. Hynes, T. C. O'Riordan, C. A. Combs, J. P. McCoy Jr, F. Bunz, J.-G. Kang and P. M. Hwang, *Nature communications*, 2010, **1**, 5.
70. J. A. Thomas, R. N. Buchsbaum, A. Zimniak and E. Racker, *Biochemistry*, 1979, **18**, 2210-2218.
71. C. Hille, M. Lahn, C. Dosche and F. Koberling, *Application Note*, 2008.
72. I. Canton and G. Battaglia, *Chemical Society Reviews*, 2012, **41**, 2718-2739.
73. T. Yoshimori, A. Yamamoto, Y. Moriyama, M. Futai and Y. Tashiro, *Journal of Biological Chemistry*, 1991, **266**, 17707-17712.
74. F. Pampaloni, E. G. Reynaud and E. H. Stelzer, *Nature reviews Molecular cell biology*, 2007, **8**, 839-845.
75. B. A. Reynolds and S. Weiss, *science*, 1992, **255**, 1707-1710.
76. G. Mehta, A. Y. Hsiao, M. Ingram, G. D. Luker and S. Takayama, *Journal of Controlled Release*, 2012, **164**, 192-204.
77. R. I. Dmitriev, A. V. Zhdanov, Y. M. Nolan and D. B. Papkovsky, *Biomaterials*, 2013, **34**, 9307-9317.
78. R. I. Dmitriev, A. V. Kondrashina, K. Koren, I. Klimant, A. V. Zhdanov, J. M. Pakan, K. W. McDermott and D. B. Papkovsky, *Biomaterials Science*, 2014, **2**, 853-866.
79. A. Lau and M. Tymianski, *Pflügers Archiv-European Journal of Physiology*, 2010, **460**, 525-542.

80. A. V. Kondrashina, R. I. Dmitriev, S. M. Borisov, I. Klimant, I. O'Brien, Y. M. Nolan, A. V. Zhdanov and D. B. Papkovsky, *Advanced Functional Materials*, 2012, **22**, 4931-4939.

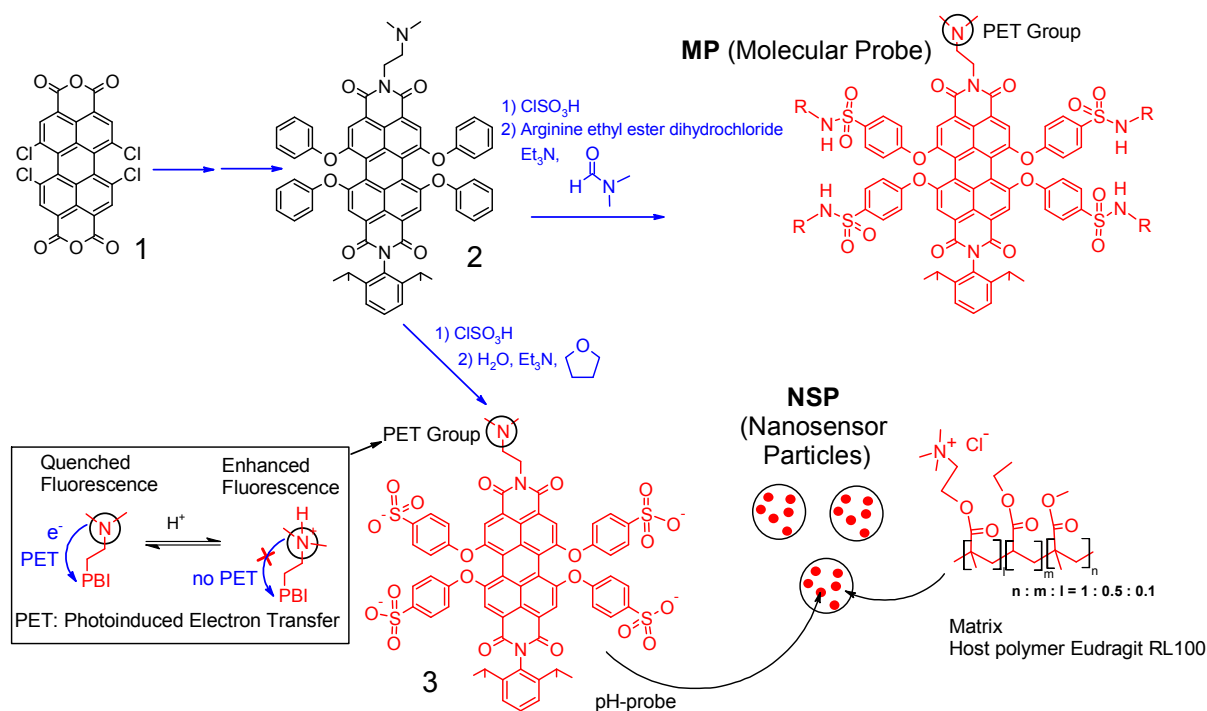
ARTICLE

Tables and figures

Table 1: Fluorescence lifetimes (calculated as stated in the experimental part) of pH-probes in different cell lines measured by FLIM microscopy at 25°C.

Probe	Environment	Average fluorescence lifetime [ns]		Half-width of lifetime distribution [ns]	
		pH 4.4	pH 8.0	pH 4.4	pH 8.0
NSP	MEF cells	4.73	3.68	0.56	0.32
	HCT116 wild type cells	4.58	3.68	0.53	0.41
	HCT116 SCO ₂ (-/-) cells	4.82	3.75	0.31	0.60
	Caco-2 cells	4.68	3.48	0.52	0.47
MP	MEF cells	3.86	2.82	1.43	0.55
	HCT116 wild type cells	4.31	3.19	0.73	0.85
	HCT116 SCO ₂ (-/-) cells	3.51	2.92	0.81	0.91
	Caco-2 cells	4.06	3.56	1.34	1.33
BCECF	MEF cells	3.79	3.64	0.22	0.29

FIGURES

**Figure 1:** Structures of NSP and MP.

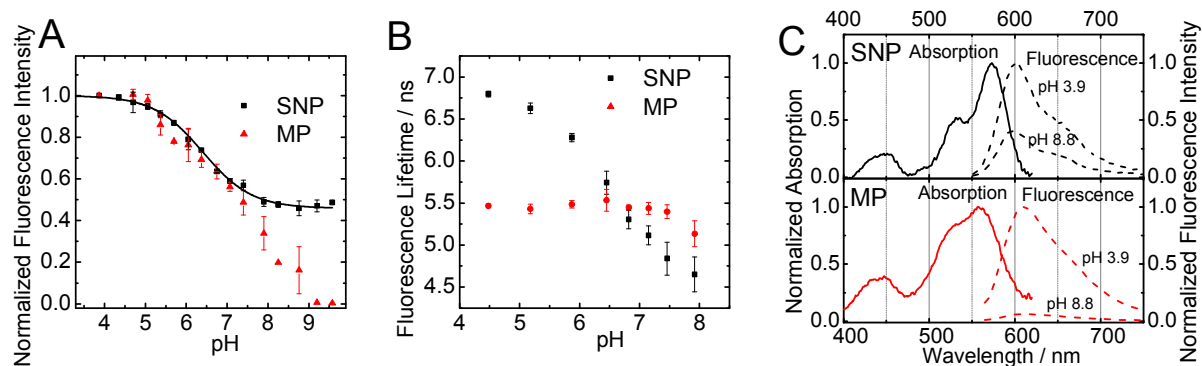


Figure 2: Photophysical properties of NSP (5 g l⁻¹) and MP (0.5 μM) in aqueous buffer at 25°C. **A:** pH calibration curves based on fluorescence intensity; **B:** Calibration based on fluorescence lifetime; **C:** Absorption and fluorescence emission (excited at 550 nm) spectra.

Journal Name

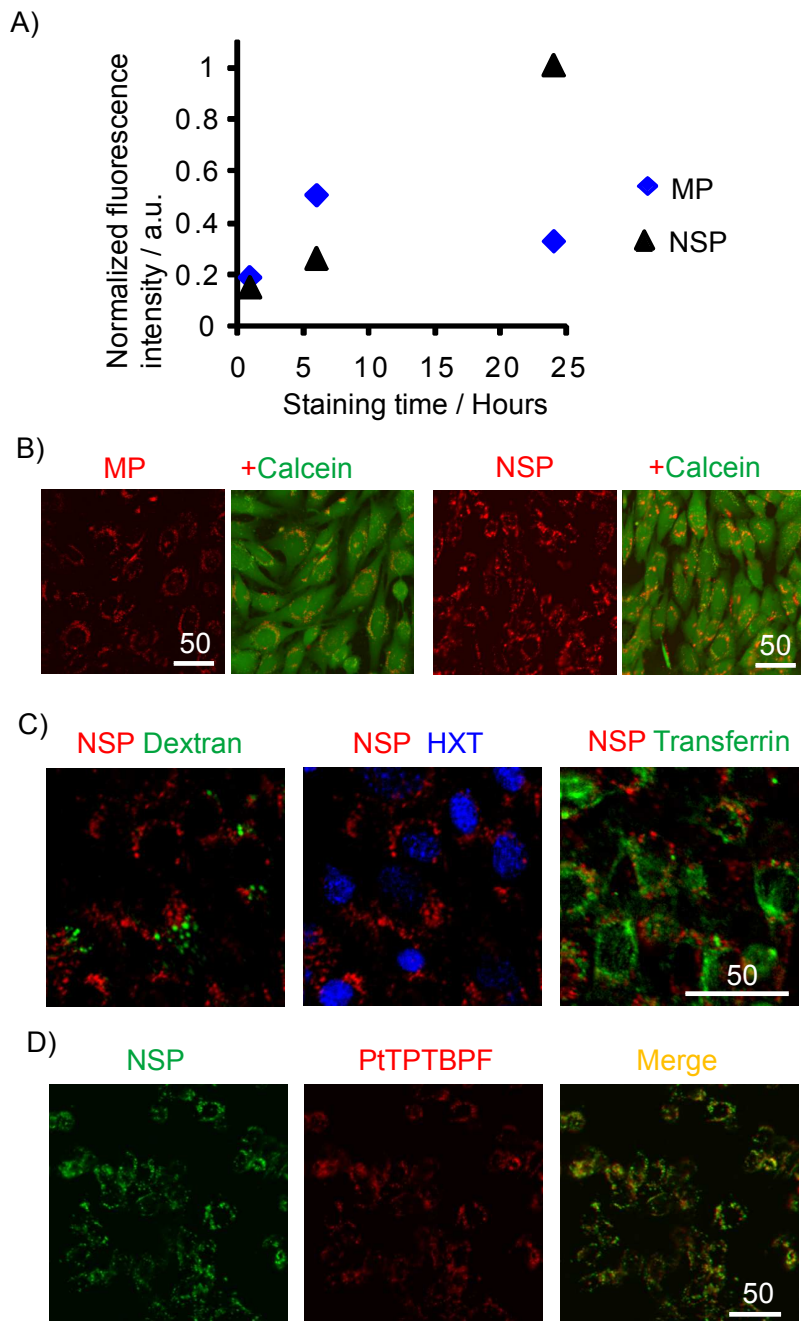


Figure 3: Cell staining properties with MEF cells. **A:** Kinetics of cell staining (0 – 24 h). Cells were incubated with probe, washed and imaged on fluorescence microscope and then their brightness in cells was quantified; **B:** Confocal images showing localization of **NSP** and **MP** in the cell, counter-stained with Calcein Green (cytosolic stain); **C:** Co-localization of **NSP** with markers of macropinosomes (Dextran 10,000), nuclei (HXT) and clathrin-mediated endosomes (transferrin); **D:** Co-localization of **NSP** with platinum(II)-*meso*-tetra(4-fluorophenyl)tetrabenzoporphyrin (PtTPTBPF) in RL100. Scale bars are in μm .

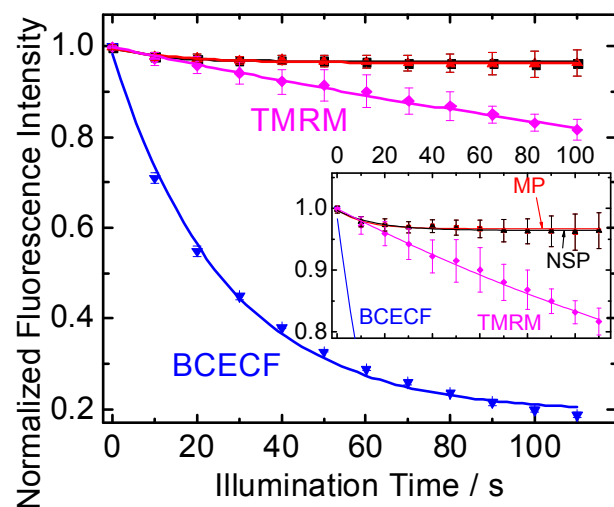


Figure 4: Photostability of NSP and MP (590 nm exc.), BCECF (470 nm exc.) and TMRM (590 nm exc.) in cultured MEF cells, under continuous illumination on a wide-field fluorescence microscope.

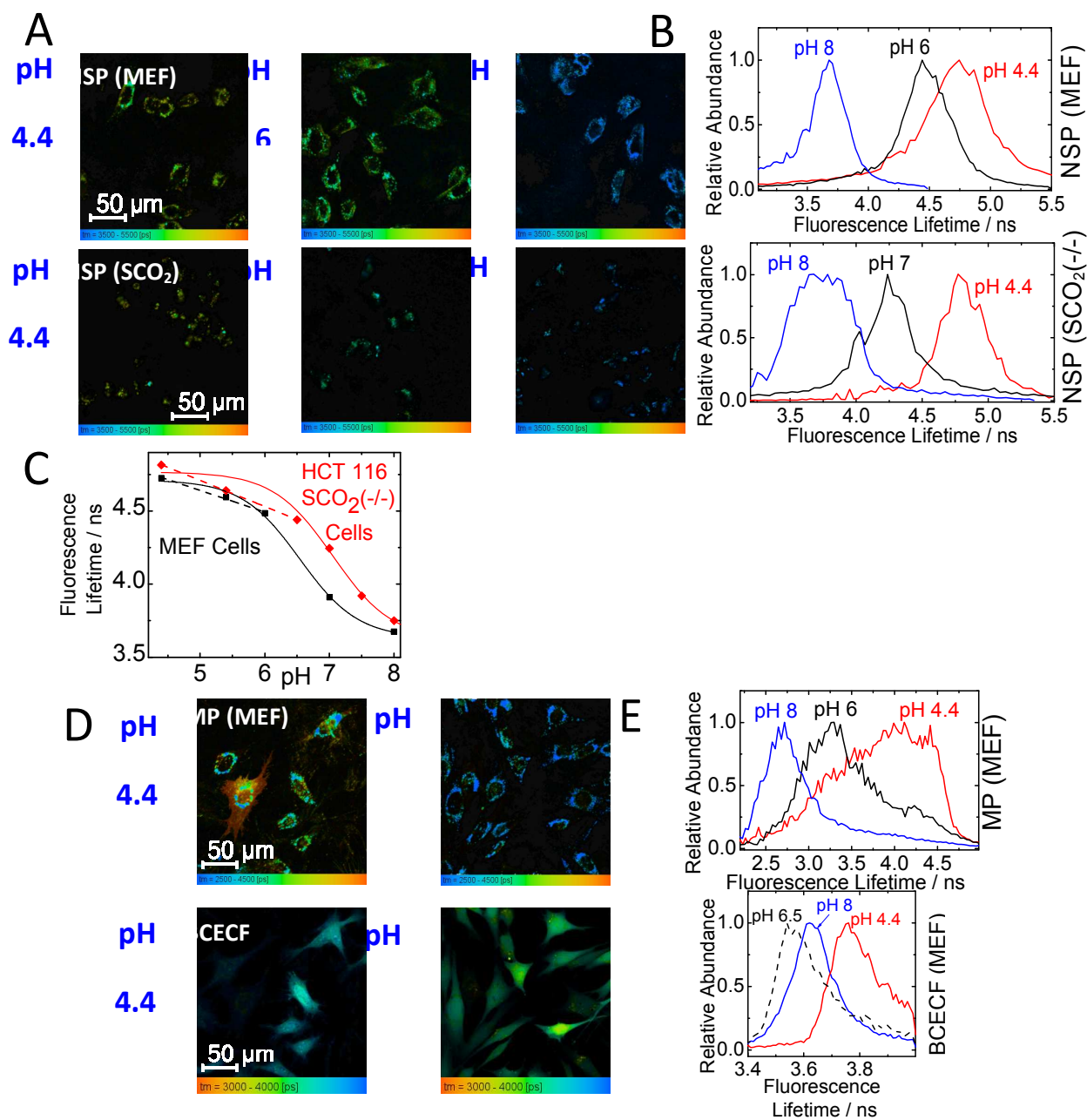


Figure 5: Confocal TCSPC-FLIM of permeabilized cells (MEF and SCO₂(-/-)), performed at 25°C. **A:** False-colour images of cells stained with NSP, permeabilized with nigericin and exposed to buffers of different pH; **B:** Corresponding distributions of lifetimes within the images; **C:** pH calibration curves (sigmoidal and linear) calculated from the distributions shown in B; **D:** Images of cells stained with MP and BCECF; **E:** Corresponding lifetime distributions.

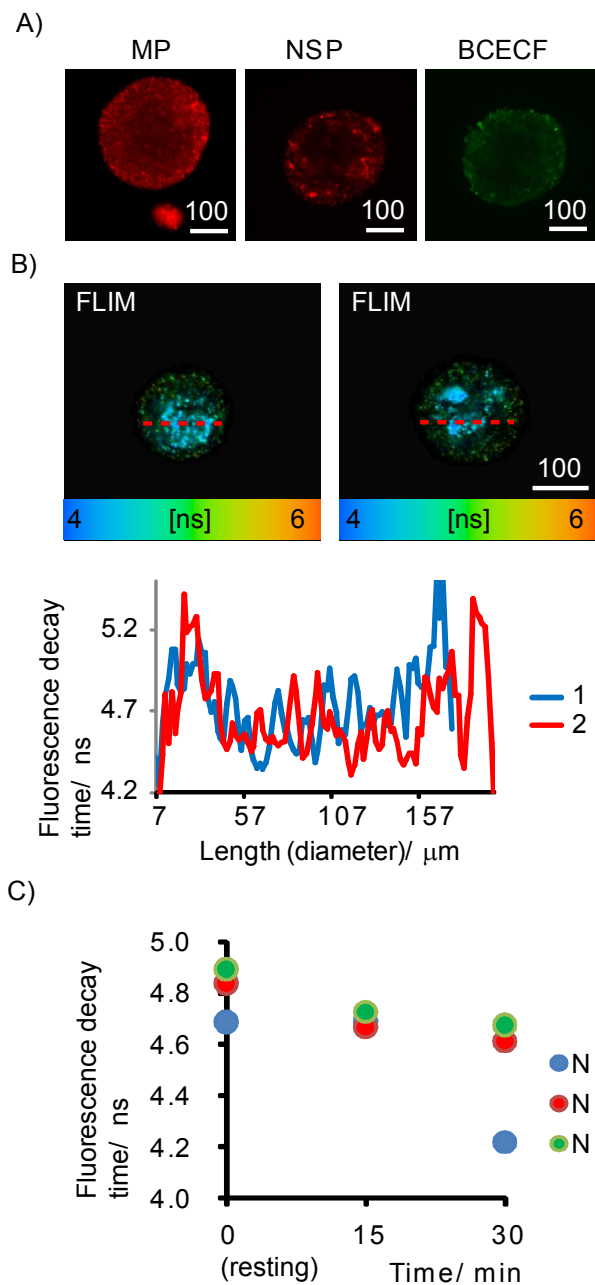


Figure 6: FLIM pH imaging with neurospheres cultured for 4 days in vitro (DIV). **A:** Typical images for neurospheres stained with **NSP** ($5 \mu\text{g ml}^{-1}$, days 1, 3), **MP** ($2 \mu\text{M}$, 24 h) and **BCECF** ($2 \mu\text{M}$, 24 h). Each image represents a single optical section across selected spheroids; **B:** False-color FLIM images of neurospheres stained with **NSP** (top) and line profiles (indicated with red dashed lines) across the spheroids (bottom); **C:** Averaged lifetime values within cores of spheroid under resting (0) and stimulated conditions (15, 30 min, 2 mM sodium glutamate), for 3 different spheroids. Scale bar is in μm .

